The JCMT Gould Belt Survey: low-mass protoplanetary discs from a SCUBA-2 census of NGC 1333

P. Dodds,[1] J. S. Greaves,[1] A. Scholz,[1][*] J. Hatchell,[2] W. S. Holland[3]
and the JCMT Gould Belt Survey Team[3][†]

[1]*SUPA, School of Physics & Astronomy, University of St Andrews, North Haugh, St Andrews, Fife KY16 9SS, UK*
[2]*Physics and Astronomy, University of Exeter, Stocker Road, Exeter EX4 4QL, UK*
[3]*UK Astronomy Technology Centre, Royal Observatory, Blackford Hill, Edinburgh EH9 3HJ, UK*

ABSTRACT

NGC 1333 is a 1–2 Myr old cluster of stars in the Perseus molecular cloud. We used 850 μm data from the Gould Belt Survey with SCUBA-2 on the James Clerk Maxwell Telescope to measure or place limits on disc masses for 82 Class II sources in this cluster. Eight disc candidates were detected; one is estimated to have mass of about 9 $M_{\rm Jup}$ in dust plus gas, while the others host only 2–4 $M_{\rm Jup}$ of circumstellar material. None of these discs exceeds the threshold for the 'minimum mass solar nebula' (MMSN). This reinforces previous claims that only a small fraction of Class II sources at an age of 1–2 Myr have discs exceeding the MMSN threshold and thus can form a planetary system like our own. However, other regions with similarly low fractions of MMSN discs (IC 348, UpSco, σ Ori) are thought to be older than NGC 1333. Compared with coeval regions, the exceptionally low fraction of massive discs in NGC 1333 cannot easily be explained by the effects of UV radiation or stellar encounters. Our results indicate that additional environmental factors significantly affect disc evolution and the outcome of planet formation by core accretion.

Key words: planets and satellites: formation – protoplanetary discs – stars: formation – stars: pre-main-sequence.

1 INTRODUCTION

Over 1000 exoplanet detections have now been claimed (e.g. exoplanet.eu), ranging from single planets to multiobject systems of varied numbers and masses. Davis (2005) has calculated that, based on the rocky content of the Solar system, at least 20 $M_{\rm Jup}$ of gas plus dust are required in a protoplanetary disc to make the Solar system planets – the minimum mass solar nebula (MMSN). Older estimates of the MMSN are in the range of 10–100 $M_{\rm Jup}$ (Weidenschilling 1977).

Current searches are finding numerous low-mass planets, in particular around low-mass stars, and close analogues to the Sun's system of planets may be uncommon. For example, Zechmeister et al. (2013) estimate the frequency of giant planets with periods smaller than 10 yr around solar-like stars to be 10 per cent, implying that exo-Jupiters are not the norm. Using microlensing results, Cassan et al. (2012) argue that the majority of solar-like stars host a Neptunian and/or super-Earth planet, whereas only around one-sixth of stars host a gas giant within 10 au. These results tend to reduce the mass requirements for circumstellar discs at early times

that can form planetary systems via core accretion. Greaves & Rice (2010) have noted that MMSN discs are uncommon around T Tauri stars, and so less substantial planetary systems than that of the Sun could be expected to form. Furthermore, Greaves & Rice (2011) suggested that dust aggregation could begin as early as the protostellar stage, and that Class 0 discs of $\gtrsim$20 $M_{\oplus}$ of dust would allow for super-Earths to be common, even if only 10 per cent of the solid material is captured into planetary cores.

We consider here whether core growth proceeds steadily with time, or whether it is also affected by environment. Star formation regions vary greatly, from spare associations such as in Taurus–Auriga up to dense clusters exemplified by the Orion nebula cluster. Wide-field surveys at wavelengths where dust emission is optically thin are thus advantageous, both for covering entire regions and for systematically identifying disc signals within complex clouds. One such programme is the Gould Belt Survey (GBS; Ward-Thompson et al. 2007), part of the Legacy Project of the James Clerk Maxwell Telescope (JCMT), which examines star formation within ∼500 pc. The SCUBA-2 (Submillimetre Common-User Bolometer Array-2) submillimetre camera (Holland et al. 2013) has produced some of the first large-scale maps of cold dust regions, and is complementary to GBSs in the infrared (IR) from *Spitzer* and *Herschel*. We present here early SCUBA-2 850 μm data for the NGC 1333 region, while Buckle et al. (in preparation), Broekhoven-Fiene et al.

[*]E-mail: as110@st-andrews.ac.uk
[†]The names of the members are given in Appendix A.

(in preparation) and Drabek-Maunder et al. (in preparation) will discuss, respectively, discs in Taurus, in Auriga and in the wider GBS survey.

NGC 1333 is a stellar cluster with about 150 young stellar objects, located at approximately 250 pc from the Sun, and within the Perseus molecular cloud. Perseus also hosts the IC 348 region, where 1.3 and 3 mm disc searches have been made by Lee, Williams & Cieza (2011) and Carpenter (2002), respectively. Scholz et al. (2013) discuss the star and brown dwarf populations of both of these regions. NGC 1333 and IC 348 have estimated ages of around 1–2 and 2–4 Myr, respectively (Bally et al. 2008). This places them within the age bracket of <1 to 5 Myr, where many young stars host cold discs. The *Spitzer* survey of NGC 1333 by Gutermuth et al. (2008) provides a catalogue for our search for submillimetre dust, especially around the Class II objects that make up two-thirds of this IR-identified population. These 'classical' T Tauri stars are expected (e.g. Lada 1987) to have more substantial discs than the remnants around Class III weak-line sources, without the confusion of circumstellar envelopes that dominate in Class I/0 protostellar systems.

2 DATA AND ANALYSIS

The observations for NGC 1333 were among the first made with SCUBA-2 at the JCMT. The data used in this paper consist of 850 μm scan maps made for the GBS between 2010 February 21 and March 7. The same data set is already discussed in Hatchell et al. (2013). Data were taken in the 'shared risk' campaign; only one sub-array of the final four was available during this campaign. The flux conversion factor was 653 ± 49 Jy beam^{-1} pW^{-1}. The weather conditions were favourable, with 225 GHz opacity of $\tau_{225} = 0.05$–0.07. Two overlapping circular regions with 15 arcmin diameter were fully scanned, offset by 10 arcmin the north and south from RA(2000) = 03^{h}29^m, Dec.(2000) = 31°18′, which is close to the centre of the cluster (Scholz et al. 2012). The 4 arcmin borders around these regions were scanned at lower sensitivity.

The map-mosaic reduction has been optimized to search for dust-disc candidates that are point-like within a 14 arcsec beam. As the cloud emission imposes a high dynamic range of fluxes, the mosaic was self-subtracted with a version smoothed over a Gaussian of 32 arcsec full width at half-maximum (FWHM). This produces some 'bowl' effects alongside the bright cloud filaments, but helps in disc identification by flattening the background. The basic map processing also includes a masking step, in which regions of low signal-to-noise are set to zero, in order to optimize the filtering out of artefacts from the scanning process. This masking could potentially result in missing any discs that are well separated from the cloud filaments. The smoothing scale of 32 arcsec was chosen to effectively remove background structures; changing this scale to 24 or 40 arcsec changes the resulting fluxes by less than 10 per cent.

A 300 arcmin^2 area of NGC 1333 was effectively imaged, within which lie 40 of the 94 Class II objects found by Gutermuth et al. (2008). Six of these are in areas near filaments and acutely affected by 'bowls' and are removed from the sample. The remaining 34 are typically 30 arcsec away from the 'bowls', which makes reliable aperture photometry feasible. Thus, the completeness of the submillimetre disc search is 36 per cent (34/94). For these 34 sources, the map depth is very uniform. The sensitivity at 850 μm is 7.8 mJy beam^{-1} rms, as measured from the scatter of 20 arcsec pixel boxes in the blankest map regions (see also Hatchell et al. 2013). This limit is also typical for the regions around the Class II sources covered by the map. The images shown have 4 arcsec pixels, so for

aperture photometry, the summed-and-sky-subtracted signals were converted from a Jy beam^{-1} to Jy pixel^{-1} scale. The beam area at 850 μm is 229 arcsec^2 (effective FWHM of 14.1 arcsec; Dempsey et al. 2013), which is equivalent to 14 pixels each of 4×4 arcsec dimensions.

As the discs should be unresolved, a small aperture with radius 2.5 pixels was adopted, and sky annuli spanned 1.5–2.5 times this radius. Aperture photometry for the 34 Class II sources was carried out with the tools of the GAIA package. The apertures were fixed on the peak pixel position, without automatic centroiding. Plausible disc candidates met the criteria of a compact (FWHM < 30 arcsec) flux peak located within 2 pixels (8 arcsec) of the T Tauri position. This roughly half-beam difference between the stellar position and centre of the peak pixel allows for centroiding error at low signal-to-noise, plus possible pointing drifts of about a half-pixel. The offsets of the peak-flux pixels were found to lie in random directions from the target coordinates, so pointing systematics are not significant.

As an additional step, we also checked the masked map areas which have low signal-to-noise ratio and inhomogeneous depth and are therefore not considered useful for accurate photometry. These areas cover most of the remaining Class II objects catalogued by Gutermuth et al. (2008). The map contains very few structures, but one faint point source signal is detected, at 14 mJy, in a region with an rms of 9 mJy.

3 RESULTS

Disc candidates were found down to 20 mJy, or 2.5 times the per-beam noise. However, the distribution of background signals subtracted in the annuli has a standard deviation of twice this noise, so weak cold-disc candidates on complex backgrounds need to be regarded with caution. Therefore, the aperture photometry could be misleading if there is structured emission in the annulus. To estimate the worst-case probability of a false positive, we consider a 1σ noise peak lying on a positive background fluctuation at one standard deviation, which would produce a nominal 3σ candidate (before subtracting the annulus signal). This probability is the product of two assumed-Gaussian tails, or $P = 0.159^2 = 0.025$. For a sample of 34 target positions, it is thus likely that one of the disc candidates (from $0.025 \times 34 = 0.86$) is not real. Visual checks were made to see if each candidate is a plausible compact source. The map with the detected and non-detected sources is shown in Fig. 1; the detections are listed in Table 1, along with their measured 850 μm fluxes and disc mass estimates.

The flux to disc mass calculation was performed using the formula (Sandell 2000)

$$M_{disc} = 0.0188(1200/\nu)^{3+\beta} F_\nu D^2 (e^{0.048\nu/T_{dust}} - 1), \qquad (1)$$

where distance D is in kpc (here adopted as 0.25) and the mass is in solar units. It is implicit that the gas-to-dust mass ratio is 100 and that the dust opacity at 1200 GHz is 0.1 cm^2 g^{-1}, thus making these mass estimates compatible with those of cloud cores in NGC 1333 (Sandell & Knee 2001) as well as disc studies in other regions (e.g. Andrews & Williams 2005; Mann & Williams 2009). Also from this work, we adopt a dust spectral index β of 1 (typical of the cores containing young stars) and a dust temperature of 30 K (within the range 20 K of often adopted for cold discs and the 40 K for *IRAS*-detected objects in NGC 1333). These factors yield 0.122 M$_\odot$ Jy^{-1} at 850 μm or 128 M_{Jup} Jy^{-1}. The distance estimate is uncertain by ≲20 per cent (Scholz et al. 2013) and the temperature by around one-third; hence, the disc masses are only quoted to one significant

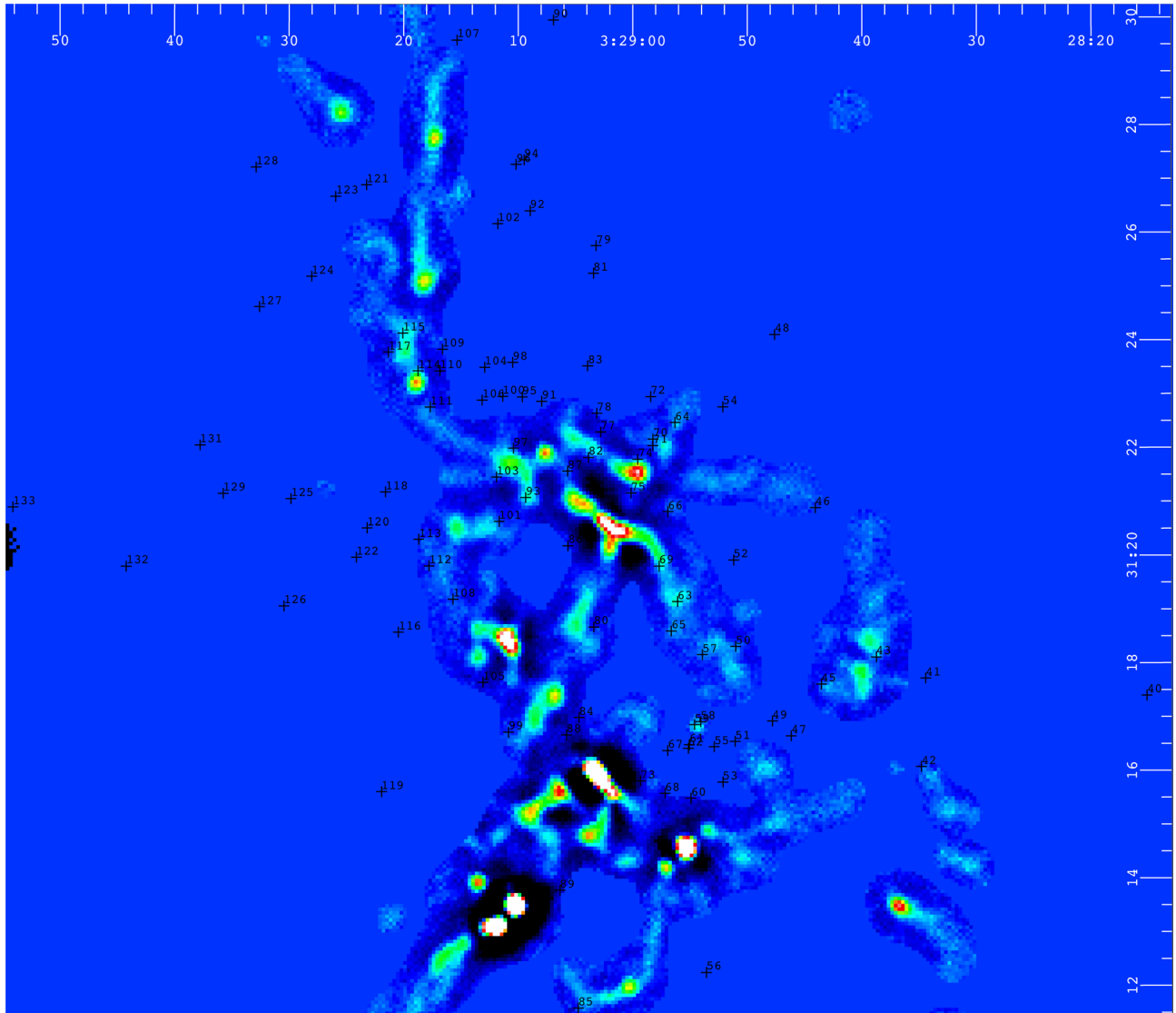**Figure 1.** Central part of 850 μm map of NGC 1333, after self-subtraction of emission of scales ≳32 arcsec (see the text). The false colour scale is linear and ranges from −15 to + 50 times the per-pixel noise, with dark blue corresponding to zero signal in masked areas of the map. Disc candidates are marked with black crosses and annotated with their numbers from the Gutermuth et al. (2008) catalogue. One candidate (#44) is outside the field of view shown here .

Table 1. NGC 1333 protoplanetary disc candidates; note that object #59 is blended with #58 (Fig. 1), so it is uncertain which source dominates the emission. Object #59 is located in the pixel of the peak emission, while #58 is 7.5 arcsec away. The first five columns list the RA-ordered object numbers, RJ coordinates, YSO names, K-band extinction and mid-IR spectral slope from Gutermuth et al. (2008). The slope is a power-law index across the *Spitzer*-IRAC 3.6–8 μm bands (not extinction corrected), with values exceeding −1.8 characterizing Class II discs. The final two columns list the SCUBA-2 850 μm flux from aperture photometry and the inferred disc mass in gas plus dust. See the text for discussion of errors.

| id#	RA,Dec.	Names	A_K	α_{IRAC}	F850 (mJy)	M_{disc} (M_{Jup})
45	03 28 43.56+31 17 36.5	ASR 127	0.41	−0.24	32	4
50	03 28 51.02+31 18 18.5	SVS 10; ASR 122; LAL 106	0.41	−0.62	31	4
59	03 28 54.61+31 16 51.3	SVS 18; ASR 43; LAL 136	0.93	−0.70	34	4
63	03 28 56.09+31 19 08.6			0.47	29	4
64	03 28 56.31+31 22 28.0	LAL 147	2.19	−0.22	22	3
65	03 28 56.64+31 18 35.7	ASR 120; LAL 150	0.80	−1.45	20	3
93	03 29 09.33+31 21 04.2	LAL 225	1.51	−0.43	74	9
111	03 29 17.66+31 22 45.2	SVS 2; LAL 283	0.31	−0.81	29	4
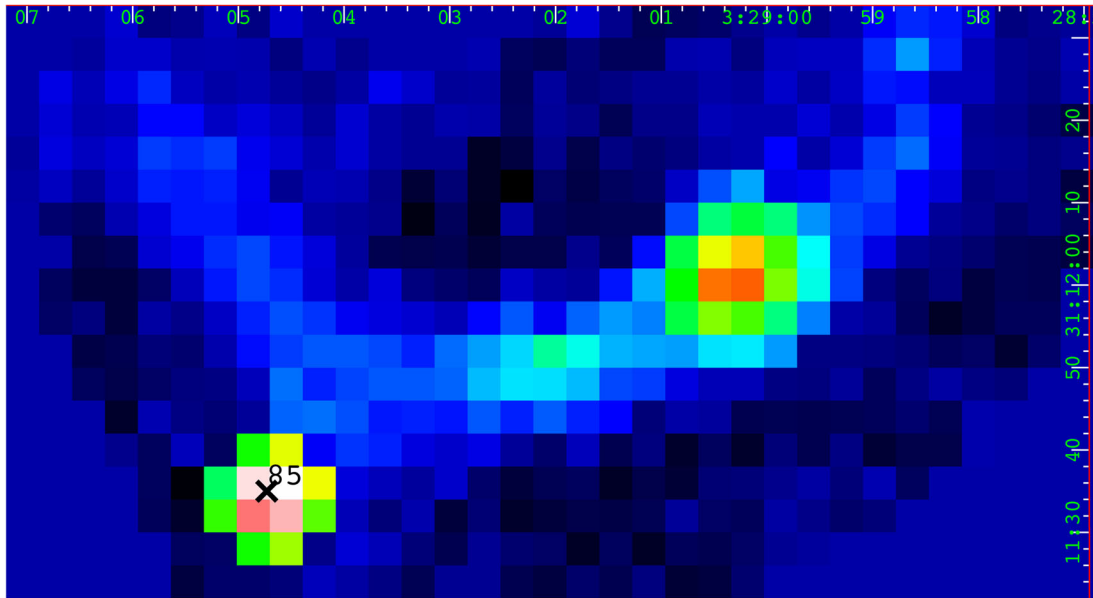
Figure 2. 850 μm image of a southern region of NGC 1333, with a fake source added. The black cross marks the position of the Class II object ASR 99 (Gutermuth-id#85) where the fake MMSN signal was superposed on a real null signal (see Section 3).

figure in Table 1. More significantly, dust already aggregated into 'pebble' sizes and above is not detected (e.g. Greaves & Rice 2011).

As pointed out in Section 2, we found one point source detection in the masked areas, outside the areas considered for reliable photometry. This source has a flux of ~16 mJy. Given this detection, an MMSN disc in these areas at 160 mJy would have been very prominent. We can therefore rule out the presence of MMSN discs in this sample of, in total, 82 Class II objects [94 are catalogued by Gutermuth et al. (2008), 6 are close to filaments and 6 are too close to the map periphery to be detected].

Thus, the result from this young region is that only one source (1 out of 34) appears to have substantial planet-forming potential. None (out of 82) has a disc with sufficient material for the MMSN. The circumstellar mass estimate for object #93 is 9 M_{Jup}, while all the other disc candidates are 2–4 M_{Jup}, well below a 20 M_{Jup} MMSN. The brightest detection is interesting because the host is a candidate sub-stellar object (Scholz et al. 2009). However, it has relatively high extinction (Table 1), so may be at an earlier stage than Class II. In addition, this source is located in a region heated by B stars which cause higher dust temperatures (Hatchell et al. 2013).

We investigated whether MMSN discs could be present, but missed owing to the high dynamic range due to the cloud filaments. Fig. 2 shows flux equivalent to 20 M_{Jup} of gas and dust injected into the map after background subtraction, at a position where there is a real Class II object but negligible 850 μm emission. The injected flux of 160 mJy was divided over a cross-shape of 12 pixels to simulate spreading over the beam. The four central pixels had twice the weight of the eight surrounding ones. Superposing this fake object into the real map resulted in a bright detection (Fig. 2). The injected flux was recovered to 85 per cent. This test confirms that a real MMSN could readily be detected even if quite close to a bright filament as in Fig. 2; within the real structure, only 0.3 per cent of map pixels are in fact brighter than this fake peak. The same procedure was repeated, but with injecting the source before background subtraction. This yielded similar results (107 per cent flux recovery).

We note that only one of the sources found in our survey (#93) is visible in the 450 μm map published by Hatchell et al. (2013). This map has a much higher rms than the map at the longer wavelength (130 mJy beam^{-1}). With the canonical value of β assumed above, all our sources are expected to have a 450 μm flux below the 2.5 σ limit. For the source #93, we estimate a relatively high submillimetre spectral slope of $\beta = 1.8$, which may confirm that this is a peculiar object, perhaps in an early evolutionary state.

4 DISCUSSION

Our results show that among 34 Class II objects in the mapped region of NGC 1333, there is one disc at 9 M_{Jup} and seven candidates of 2–4 M_{Jup}, of which one is likely to be due to noise fluctuations as discussed above. Out of a sample of 82 Class II objects, none has a disc with a mass exceeding the MMSN. The robustness test of the previous section shows that MMSN discs are unlikely to be missed, even in regions of the map with bright residual structure from cloud filaments.

In Table 2, we compare our results with those of other nearby star-forming regions, including only Class II sources (i.e. excluding embedded Class I as well as discless Class III objects). Using a variety of literature sources, we calculate the fraction of stars per region hosting discs of masses at, or exceeding, 1 MMSN, f_{MMSN}. These numbers are essentially an updated version of the data presented in Greaves & Rice (2010). In addition, we derive the fraction of stars in each region hosting discs above our detection limit of 3 M_{Jup}, f_{Mlim}. For both disc fractions, we calculate consistent 1σ binomial confidence intervals. The table includes regions with ages of 1–2 Myr (NGC 1333, ONC, Taurus, Ophiuchus, Lupus, Cha-I), 2–5 Myr (IC 348, σ Ori) and 5–10 Myr (UpSco), and thus covers the entire age range of Class II sources (see also the revised age scale; Bell et al. 2013). For most of these regions, the disc masses have been derived from submm/mm fluxes at 850 μm or 1.3 mm, using similar assumptions for the dust opacity and temperature as well as gas-to-dust ratio; the values should therefore be comparable.

Table 2. Number of Class II MMSN discs N, fraction f and 1σ confidence intervals for nearby star-forming regions.

Region	Age (Myr)	$N_{\rm MMSN}$	$f_{\rm MMSN}$ (per cent)	1σ (per cent)	$N_{\rm Mlim}$	$f_{\rm Mlim}$ (per cent)	1σ (per cent)	Reference
N1333	1–2	0/82	0	0–2	8/34	24	16–33	This paper
Lupus	1–2	2/32	6	2–14	$\geq$12/32	38	28–48	Nuernberger, Chini & Zinnecker (1997)
Cha-I	1–2	1/14	7	1–21	$\geq$6/14	43	28–59	Henning et al. (1993)
ONC	1–2	6/55	11	7–17	25/55	45	38–53	Mann & Williams (2009)
Tau-Aur	1–2	15/74	20	16–26	38/74	51	45–58	Andrews & Williams (2005)
Oph	1–2	15/69	22	17–28	$\geq$31/69	45	39–51	Andrews & Williams (2007)
IC 348	2–4	0/84	0	0–2	3/84	4	2–7	Lee et al. (2011)
σ Ori	3–5	0/297	0	0–1	$\geq$9/297[a]	3	2–4	Williams et al. (2013)
UpSco	5–10	0/37	0	0–5	1/37	3	0–9	Mathews et al. (2012)

Note: [a]The detection limit in this study is 4.5 $M_{\rm Jup}$, i.e. only slightly higher than in our paper. The quoted lower limit is therefore likely to be close to the actual value.
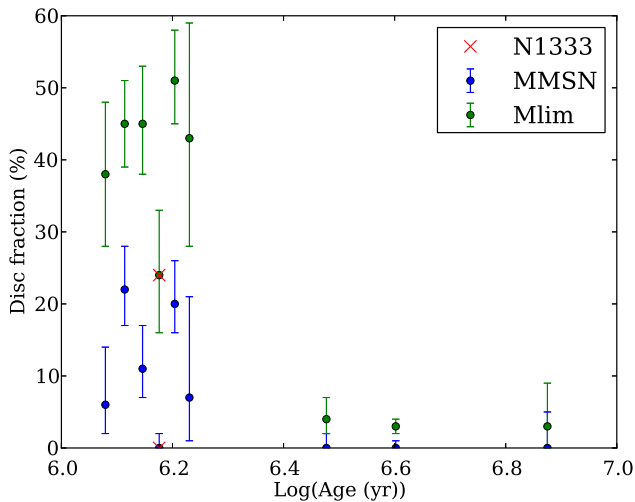

Figure 3. Percentages of Class II discs in star-forming regions, with masses above MMSN (blue) and above 3 $M_{\rm Jup}$ (our detection limit, green). Error bars are binomial 1σ confidence intervals. See Table 2 for references. For the regions with ages between 1 and 2 Myr, the ages shown in the plot are arbitrary and have been chosen to allow for a clear presentation. The percentages for NGC 1333 are marked with red crosses.

For many regions included in Table 2, the submm/mm census is reasonably complete. This includes Ophiuchus, Taurus–Auriga, IC 348 and σ Ori. For other regions, however, the disc fractions are calculated from an incomplete sample, which raises the issue of potential biases. In Cha-I, the value for the MMSN fraction is based on the more than 20-yr-old study by Henning et al. (1993). Their photometry is not homogeneous (the noise varies by a factor of 4) and could be biased. However, a more recent assessment of disc masses in Cha-I based on *Herschel* fluxes finds $f_{\rm MMSN}$ of 2–7 per cent (Rodgers-Lee et al. 2014), which is in line with the previous value. In NGC 1333, Lupus and UpSco, the sample sizes are also small (<40), but are without any known bias. In NGC 1333, we may miss some discs near the filaments, as pointed out in Section 2. Strong background emission such as in these filaments is a limitation of many submm/mm surveys in star-forming regions. For example, the fields observed in the ONC (Mann & Williams 2009) and IC 348 (Lee et al. 2011) deliberately avoid localized regions with cloud emission.

The disc fractions in Table 2 are plotted versus age of the region in Fig. 3. In general, only few discs have sufficient dust mass for the formation of massive planetary cores. For example, our 2–4 $M_{\rm Jup}$

candidates in NGC 1333 include only about 10 $M_\oplus$ of solids, spread over the entire disc. These results are in agreement with the findings from exoplanet surveys (see Section 1) which indicate that planetary systems comparable to the Solar system are the exception, and that smaller and less massive systems are more common. Nevertheless, about 20 to 50 per cent of discs at ages of 1–2 Myr still have sufficient mass to form systems with super-Earth-type planets.

The figure also demonstrates that $f_{\rm MMSN}$ and $f_{\rm Mlim}$ vary from region to region. IC 348, UpSco and σ Ori on the right-hand side of the plot contain a negligible fraction of MMSN discs and a very low fraction of discs above our mass limit. For these three regions, the fraction of massive discs is significantly lower than that for the younger regions. This has been noted before by Williams et al. (2013), Lee et al. (2011), as well as Mathews et al. (2012). In all three cases, the low fraction of massive discs is interpreted in the framework of standard viscous evolution of discs; as the objects age, the disc material is dissipated and the dust content drops. As a result, the three regions which are slightly older than the others are also found to have the lowest fraction of massive discs.

All the remaining regions should have comparable ages, around 1–2 Myr. In this group, there is still substantial spread in $f_{\rm MMSN}$ and $f_{\rm Mlim}$. NGC 1333, the region investigated here, has the lowest value for $f_{\rm MMSN}$ and $f_{\rm Mlim}$. The disc fraction in NGC 1333 is significantly lower than that in Taurus, Ophiuchus and the ONC (i.e. with non-overlapping 1σ confidence intervals), and still somewhat lower than that in Lupus and Cha-I. Here, age cannot be invoked as an explanation. Stars in NGC 1333 either already have partially formed planetary systems (i.e. a lot of mass is already bound in large grains and planetesimals) or they will form systems with less massive planets than other regions. Note that this conclusion is robust against uncertainties in distance or dust temperature; even increasing all our disc masses by 50 per cent would not affect the outcome.

Thus, this comparison indicates that there are secondary factors, apart from age, that affect the fraction of massive discs at Class II stage and thus the potential for planet formation. In the following, we investigate four possible candidates for such secondary factors.

(1) *Dynamical interactions in dense stellar clusters:* if this factor were to play a role, we would expect *stronger* effects in the ONC, as the ONC has higher stellar density than NGC 1333 [$\sim$400 pc^{-3} versus <100 pc^{-3}; see Huff & Stahler (2006) and Scholz et al. (2013)]. However, stellar encounters are unlikely to play a significant role in the disc evolution in the ONC (e.g. Scally & Clarke 2001), and therefore even less so in NGC 1333. Recently, Rosotti et al. (2014) use hydrodynamical simulations to show that stellar encounters limit disc radii (but not necessarily disc masses) for stellar

densities exceeding $2–3 \times 10^3$ pc^{-1}, more than one order of magnitude higher than in NGC 1333.

(2) *Photoevaporation in the UV-radiation field of nearby OB stars:* as in the previous scenario, we would expect stronger effects in the ONC, which harbours more OB stars than NGC 1333. Mann et al. (2014) find that the ONC is lacking massive discs only in the vicinity of the O star θ^1 Ori C, within 0.03 pc, whereas in other regions the disc mass distribution is similar to regions like Taurus. This is explained by the effect of the UV radiation on the discs. NGC 1333 does not harbour any O stars, but two B stars (B5 and B8; see Hatchell et al. 2013). However, our survey extends to distances of 0.5 pc from them, and we do not find any massive discs. Hence, this scenario does not seem applicable to NGC 1333.

(3) *Metallicity:* the estimates for the MMSN assume a composition as found in the Solar system. A star-forming environment with a chemical composition different from the solar nebula could yield different planetary systems. To our knowledge, the metallicity for stars in NGC 1333 is not constrained yet; this scenario needs further investigation.

(4) *Grain growth:* it is conceivable that grains grow faster in NGC 1333. In fact, several young protostars in NGC 1333 have been identified with MMSN-mass discs (Greaves & Rice 2011). Thus, at the very early stage, massive discs do exist, but fast coagulation of grains may prevent their detection at Class II stage. At this point, however, it is not clear what could cause anomalously fast grain growth. To explore this scenario further, the discs in NGC 1333 need to be observed at mm and cm wavelengths to constrain the grain properties.

5 SUMMARY AND CONCLUSION

This is the first wide-field study searching for T Tauri discs in the submm/mm within the NGC 1333 star formation region. Aperture photometry was performed on background-subtracted maps. Eight disc candidates were identified. One has mass of about one half MMSN, with the rest only hosting a few Jupiter masses of material. The fraction of discs with MMSN mass or more in NGC 1333 is thus negligible, while the fraction of discs with masses above our limit of ~ 3 M_{Jup} is 24 per cent.

We compare these values to disc fractions for other star-forming regions and find that an anomalously low fraction of Class II objects in NGC 1333 has discs with masses exceeding the MMSN threshold and discs with masses exceeding our detection limit. We rule out age, dynamical interactions and photoevaporation by nearby OB stars as possible reasons for the lack of massive discs in NGC 1333. Other options to explain this result include an anomalous metallicity or faster grain growth. Our study thus raises the possibility that environmental factors (beyond age) can have a significant impact on the evolution of the discs and the outcome of planet-forming processes.

ACKNOWLEDGEMENTS

REFERENCES

Andrews S. M., Williams J. P., 2005, ApJ, 631, 1134
Andrews S. M., Williams J. P., 2007, ApJ, 671, 1800
Bally J., Walawender J., Johnstone D., Kirk H., Goodman A., 2008, in Reipurth B., ed., ASP Monograph Publications Vol. 4, Handbook of Star Forming Regions: The Northern Sky. Astron. Soc. Pac., San Francisco, p. 308
Bell C. P. M., Naylor T., Mayne N. J., Jeffries R. D., Littlefair S. P., 2013, MNRAS, 434, 806
Carpenter J. M., 2002, AJ, 124, 1593
Cassan A. et al., 2012, Nature, 481, 167
Davis S. S., 2005, ApJ, 627, L153
Dempsey J. T. et al., 2013, MNRAS, 430, 2534
Greaves J. S., Rice W. K. M., 2010, MNRAS, 407, 1981
Greaves J. S., Rice W. K. M., 2011, MNRAS, 412, L88
Gutermuth R. A. et al., 2008, ApJ, 674, 336
Hatchell J. et al., 2013, MNRAS, 429, L10
Henning T., Pfau W., Zinnecker H., Prusti T., 1993, A&A, 276, 129
Holland W. S. et al., 2013, MNRAS, 430, 2513
Huff E. M., Stahler S. W., 2006, ApJ, 644, 355
Lada C. J., 1987, in Peimbert M., Jugaku J., eds, Proc. IAU Symp. 115, Star Forming Regions. Reidel, Dordrecht, p. 1
Lee N., Williams J. P., Cieza L. A., 2011, ApJ, 736, 135
Mann R. K., Williams J. P., 2009, ApJ, 694, L36
Mann R. K. et al., 2014, ApJ, 784, 82
Mathews G. S., Williams J. P., Ménard F., Phillips N., Duchêne G., Pinte C., 2012, ApJ, 745, 23
Nuernberger D., Chini R., Zinnecker H., 1997, A&A, 324, 1036
Rodgers-Lee D., Scholz A., Natta A., Ray T., 2014, MNRAS, 443, 1587
Rosotti G. P., Dale J. E., de Juan Ovelar M., Hubber D. A., Kruijssen J. M. D., Ercolano B., Walch S., 2014, MNRAS, 441, 2094
Sandell G., 2000, A&A, 358, 242
Sandell G., Knee L. B. G., 2001, ApJ, 546, L49
Scally A., Clarke C., 2001, MNRAS, 325, 449
Scholz A., Geers V., Jayawardhana R., Fissel L., Lee E., Lafreniere D., Tamura M., 2009, ApJ, 702, 805
Scholz A., Jayawardhana R., Muzic K., Geers V., Tamura M., Tanaka I., 2012, ApJ, 756, 24
Scholz A., Geers V., Clark P., Jayawardhana R., Muzic K., 2013, ApJ, 775, 138
Ward-Thompson D. et al., 2007, PASP, 119, 855
Weidenschilling S. J., 1977, Ap&SS, 51, 153
Williams J. P. et al., 2013, MNRAS, 435, 1671
Zechmeister M. et al., 2013, A&A, 552, A78

APPENDIX A: THE JCMT GBS TEAM

The current members of the JCMT GBS team are P. Bastien, S. F. Beaulieu, D. S. Berry, H. Broekhoven-Fiene, J. Buckle, H. Butner, M. Chen, H. Christie, A. Chrysostomou, A. Chrysostomou, S. Coude, M. J. Currie, C. J. Davis, J. Di Francesco, E. Drabek-Maunder, A. Duarte-Cabral, M. Fich, J. Fiege, P. Friberg, R. Friesen, G. A. Fuller, S. Graves, J. Greaves, J. Gregson, J. Hatchell, M. R. Hogerheijde, W. Holland, T. Jenness, D. Johnstone, G. Joncas, H. Kirk, J. M. Kirk, L. B. G. Knee, S. Mairs, K. Marsh, B. C. Matthews, G. Moriarty-Schieven, J. C. Mottram, K. Pattle, J. Rawlings, J. Richer, D. Robertson, E. Rosolowsky, D. Rumble, S. Sadavoy, C. Salji, H. Thomas, M. Thompson, N. Tothill, S. Viti, D. Ward-Thompson, G. J. White, C. D. Wilson, J. Wouterloot, J. Yates and M. Zhu.

This paper has been typeset from a TEX/LATEX file prepared by the author.